



# Excellent dielectric constants observed in heterogeneous conduction Ba(Zr<sub>0.25</sub>Ti<sub>0.75</sub>)O<sub>3</sub> ceramics doped with Sr(Fe<sub>0.5</sub>Nb<sub>0.5</sub>)O<sub>3</sub>

Pharatree Jaita<sup>1</sup> · Lalita Tawee<sup>1</sup> · Ratabongkot Sanjoom<sup>2</sup> · Chamnan Randorn<sup>3</sup> · Komsanti Chokethawai<sup>1</sup> · Gobwute Rujijanagul<sup>1</sup>

Received: 29 November 2017 / Accepted: 23 August 2018 / Published online: 19 September 2018  
© Springer Science+Business Media, LLC, part of Springer Nature 2018

## Abstract

The (1-*x*)Ba(Zr<sub>0.25</sub>Ti<sub>0.75</sub>)O<sub>3</sub>-*x*Sr(Fe<sub>0.5</sub>Nb<sub>0.5</sub>)O<sub>3</sub> or (1-*x*)BZT-*x*SFN ceramics have been fabricated via a solid-state reaction technique. All ceramics exhibit a pure phase perovskite with cubic symmetry. The addition of a small amount of SFN (*x* = 0.1) produces an obvious change in dielectric behavior. Very high dielectric constants ( $\epsilon_r > 164,000$  at 1 kHz and temperature > 150 °C) are observed and the value is obviously higher than dielectric constants for Ba(Zr<sub>0.25</sub>Ti<sub>0.75</sub>)O<sub>3</sub> and Sr(Fe<sub>0.5</sub>Nb<sub>0.5</sub>)O<sub>3</sub> ceramics. The ferroelectric measurement data suggests that the unmodified sample exhibited a ferroelectric behavior. However, a transformation from a ferroelectric to a relaxor-like behavior is noted with increasing *x* concentration. Impedance Spectroscopy (IS) analysis indicates that the presence of excellent dielectric constants is due to the heterogeneous conduction in the ceramics after adding SFN, which can be explained in terms of the Maxwell-Wagner polarization mechanism.

**Keywords** Solid-state reaction · High dielectric constant · Ferroelectric · Perovskite

## 1 Introduction

For many years, barium zirconium titanate or Ba(Zr<sub>*x*</sub>Ti<sub>1-*x*</sub>)O<sub>3</sub> and BZT-based ceramics have received considerable attention from many researchers due their interesting electrical properties and the lack of lead pollution during processing [1–7]. BZT ceramics exhibit high electrical performances such as high dielectric constant [2], and ferroelectric [5] and piezoelectric properties [4]. This leads to their use as a replacement for lead-based ceramics such as lead zirconate titanate or Pb(Zr, Ti)O<sub>3</sub>, PZT. The BZT ceramics can be formed by the substitution of Zr ions at the B-site in BaTiO<sub>3</sub> lattices [1–7], which significantly changes the electrical properties, and structural and diffuse phase transition [6, 7]. Furthermore, some compositions of BZTs present many interesting properties such as Ba(Zr<sub>0.07</sub>Ti<sub>0.93</sub>)O<sub>3</sub>

exhibiting a high dielectric constant and good piezoelectric properties. BZT with the composition of 0.25 < *x* ≤ 0.85 exhibits a strong frequency dispersion and a broad temperature peak of the dielectric constant-temperature curve [3, 6]. The solid solution of BZT with other materials showed many interesting properties. For example, (1-*x*)Ba(Zr<sub>0.07</sub>Ti<sub>0.93</sub>)O<sub>3</sub>-*x*Ba(Fe<sub>0.5</sub>Nb<sub>0.5</sub>)O<sub>3</sub> or (1-*x*)BZT-*x*BFN presents very high dielectric properties [8]. The 0.9BZT-0.1BFN sample presents a dielectric-frequency dependence with low loss tangent ( $\tan \delta < 0.07$  at the frequency of 10 kHz). For the composition of *x* > 0.2, the dielectric data exhibits a broad dielectric constant-temperature curve with a giant dielectric constant characteristic. In addition, a high dielectric constant >50,000 (at 10 kHz and temperature > 150 °C) was reported for the *x* = 0.9 sample [8].

Sr(Fe<sub>0.5</sub>Nb<sub>0.5</sub>)O<sub>3</sub> (SFN) ceramics are interestingly high dielectric materials due to their high dielectric constants. The dielectric constants of these materials are in the order of 10<sup>3</sup>–10<sup>4</sup> over wide frequency and broad temperature ranges [9, 10]. SFN ceramics also exhibit a strong dielectric-frequency dispersion, similar to other giant dielectric ceramics such as Ba(Fe<sub>0.5</sub>Nb<sub>0.5</sub>)O<sub>3</sub> [11], A(Fe<sub>1/2</sub>Ta<sub>1/2</sub>)O<sub>3</sub> [A = Ba, Sr, Ca] [12, 13], and CaCu<sub>3</sub>Ti<sub>4</sub>O<sub>12</sub> [14]. The high dielectric behavior of SFN and many giant dielectric ceramics have been explained in terms of the Maxwell-Wagner polarization mechanism [11]. Furthermore, solid solutions between SFN and other materials present many interesting properties. For

✉ Gobwute Rujijanagul  
rujijanagul@yahoo.com

<sup>1</sup> Department of Physics and Materials Science, Faculty of Science, Chiang Mai University, Chiang Mai 50200, Thailand

<sup>2</sup> Department of Applied Science and Biotechnology, Faculty of Agro-Industrial Technology, Rajamangala University of Technology Tawan-ok Chanthaburi Campus, Chanthaburi 22210, Thailand

<sup>3</sup> Department of Chemistry, Faculty of Science, Chiang Mai University, Chiang Mai 50200, Thailand

example, SFN-BaTiO<sub>3</sub> ceramics showed a very high dielectric constant and a very high relative dielectric tenability [15].

Many authors have reported that properties of BZT (beside the dielectric properties) can be improved by doping or forming solid-solution with other materials [16, 17]. For example, Ba(Zr<sub>0.07</sub>Ti<sub>0.93</sub>)O<sub>3</sub> doped with B<sub>2</sub>O<sub>3</sub> presented a high electric field induced strain [16]. The solid solution between BZT and BCT (Ba<sub>0.7</sub>Ca<sub>0.3</sub>)TiO<sub>3</sub> showed high pyroelectricity [17]. Therefore, it would be interesting to form a new solid-solution between BZT and other materials such as SFN because BZT ceramics presents many interesting properties and SFN ceramics exhibit high dielectric constants with the strong dielectric-frequency dispersion. Furthermore, properties of the solid-solution of BZT and SFN have not been investigated to our knowledge. The aim of this work is therefore to investigate the properties of the solid solution between BZT and SFN ceramics. In the present work, BZT with a composition of Ba(Zr<sub>0.25</sub>Ti<sub>0.75</sub>)O<sub>3</sub> was selected for the solid-solution formation. Many properties of the solid-solution were studied and discussed.

## 2 Experimental

The solid state reaction process was applied to synthesize the (1-x)Ba(Zr<sub>0.25</sub>Ti<sub>0.75</sub>)O<sub>3</sub>-xSr(Fe<sub>0.5</sub>Nb<sub>0.5</sub>)O<sub>3</sub> or (1-x)BZT-xSFN ceramics with x = 0, 0.1, 0.3 and 0.5 mol fraction. The starting powders of BaCO<sub>3</sub>, ZrO<sub>2</sub>, TiO<sub>2</sub>, SrCO<sub>3</sub>, Fe<sub>2</sub>O<sub>3</sub> and Nb<sub>2</sub>O<sub>5</sub> were used as the starting raw materials. All carbonate powders were first dried at 120°C for 24 h in order to remove any moisture. The raw materials of (1-x)BZT-xSFN were stoichiometrically weighed and mixed by ball milling in 99.9% ethanol for 24 h, and the slurry was dried using an oven. The mixed powders were then calcined at 1300°C for 4 h. The calcined powders were mixed with 6 wt% of a polyvinyl alcohol binder (PVA). After that, the resulting product was pressed into pellets with ~ 10 mm in diameter and ~ 1.3 mm in thickness. The obtained pellets were sintered at 1450°C for 4 h dwell time.

An X-ray diffractometer (XRD-Phillip, X-pert) was used to identify the phases present in both powders and ceramics. The Raman spectra were obtained on polished sintered pellets with a Raman spectrometer (T6400 JY, Horiba Jobin Yvon). Bulk density was measured in accordance with the Archimedes' method using distilled water as a fluid medium with ASTM standard C 373–88. Before being subjected to electrical characterization, all samples were carefully polished to 1 mm thickness to obtain a parallel scratch-free surface. Silver paste was painted onto both sides of each sample and then fired at 700°C for 30 min to form electrodes. Dielectric properties as a function of temperature (25–300°C) were carried out using a HP 4192A LCR-meter connected to a high temperature furnace

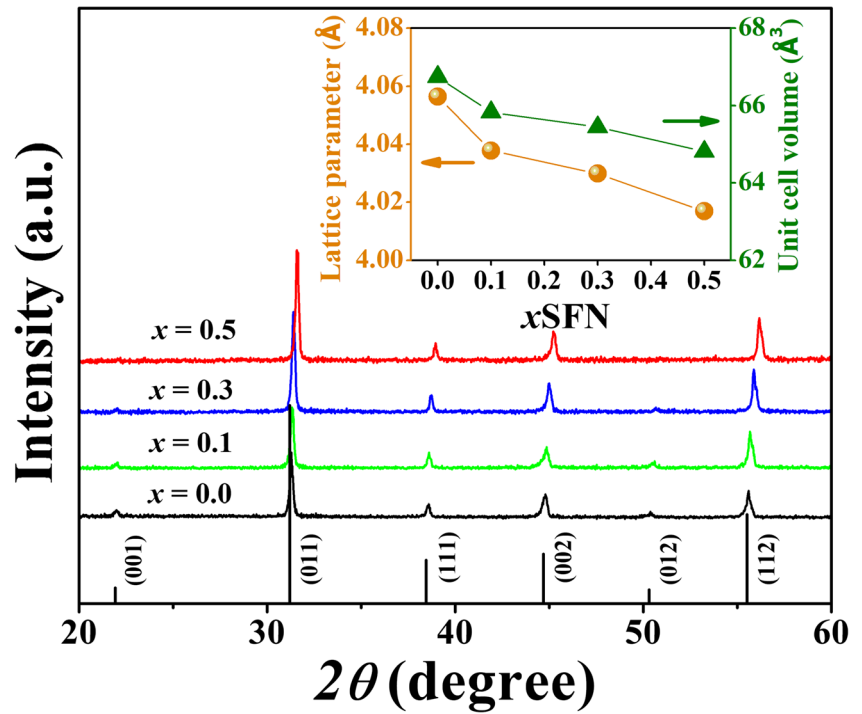
with frequencies ranging from 1 to 1000 kHz. A ferroelectric system based on Radiant Precision High Voltage Interface was used to measure the polarization-electric field (*P-E*) hysteresis loop at various temperatures. The AC electric field of 15 kV/cm and a frequency of 1 Hz were applied to each sample.

## 3 Results and discussion

The X-ray diffraction (XRD) patterns obtained from each composition of (1-x)BZT-xSFN ceramics within 2θ range of 20–60° are shown in Fig. 1. It can be seen that all XRD patterns present a single perovskite structure with no trace of secondary phases. This result suggests a complete solid solution between BZT and SFN in the (1-x)BZT-xSFN ceramics. Furthermore, the result also indicates that the synthesized solid-solution is stable and easy to form. The phase of pure BZT ceramic was indexed according to the International Centre for Diffraction Data (ICDD) file number 00–036–0019 and the symmetry of all samples was identified as cubic (at room temperature). The present XRD result agrees with data reported by previous work [18]. For the modified ceramics, the positions of all peaks shift slightly to higher 2θ angles in comparison with the unmodified BZT ceramic. The overall shift of XRD patterns is possibly attributed to the differences in ionic radii of Ba<sup>2+</sup> (1.42 Å) and Sr<sup>2+</sup> (1.26 Å) at A-site and also Zr<sup>4+</sup> (0.84 Å), Ti<sup>4+</sup> (0.74 Å), Fe<sup>3+</sup> (0.78 Å), and Nb<sup>5+</sup> (0.64 Å) at B-site of the lattice [19]. In this work, lattice parameter and unit-cell volume (at room temperature) of the samples were calculated. The values of lattice parameter and unit-cell volume as a function of SFN concentration are shown in the inset of Fig. 1. It is seen that the lattice parameter and unit-cell volume decrease with increasing the SFN concentration. The decrease in unit-cell volume indicates a distortion of crystal for the solid solution as compared to the pure BZT.

To have a further investigation of the phase formation, Raman scattering technique was employed. Raman spectra at room temperature (RT) of the studied samples are displayed in Fig. 2. The Raman spectra of the unmodified BZT ceramics correspond to Raman spectra of BZT of many previous works [20–22]. The main peaks of Raman spectra are noted at 110, 182, 258, 300, 516 and 714 cm<sup>-1</sup>, respectively. The peaks at 110 and 300 cm<sup>-1</sup> correspond to E(TO<sub>1</sub>) and E<sub>1</sub>(TO<sub>2</sub>) mode, respectively [20, 21]. The stretching modes of A<sub>1</sub>(TO<sub>1</sub>), A<sub>1</sub>(TO<sub>2</sub>) and A<sub>1</sub>(TO<sub>3</sub>) are displayed at ~ 182, 258 and 516 cm<sup>-1</sup>, respectively. Furthermore, A<sub>1</sub>(LO<sub>3</sub>) mode is noted at 714 cm<sup>-1</sup> which corresponds to zirconium (Zr) substituting on titanium (Ti) sites at B-site of the lattice [21, 22]. After adding SFN, the Raman spectra are changed, in that the main peaks shift and become broader. Furthermore, the A<sub>1</sub>(TO<sub>3</sub>) peak at 516 cm<sup>-1</sup> splits into two broad peaks. This also confirms a distortion of structure due to the SFN additive.

**Fig. 1** XRD patterns of (1- $x$ )BZT- $x$ SFN ceramics (Inset: Lattice parameter and unit cell volume as a function of SFN content)



Calculated and measured density as a function of SFN concentration is presented in Fig. 3. There is a significant change in the density value for the modified ceramics. Both calculated and measured density values decrease with

SFN concentration. This result is probably due to the lower density of SFN (5.62 g/cm<sup>3</sup>) as compared to that of BZT (6.41 g/cm<sup>3</sup>). Furthermore, the measured density curve exhibits non-linear and deviates from the calculated density

**Fig. 2** Raman spectra of the (1- $x$ )BZT- $x$ SFN ceramics at room temperature with different SFN content

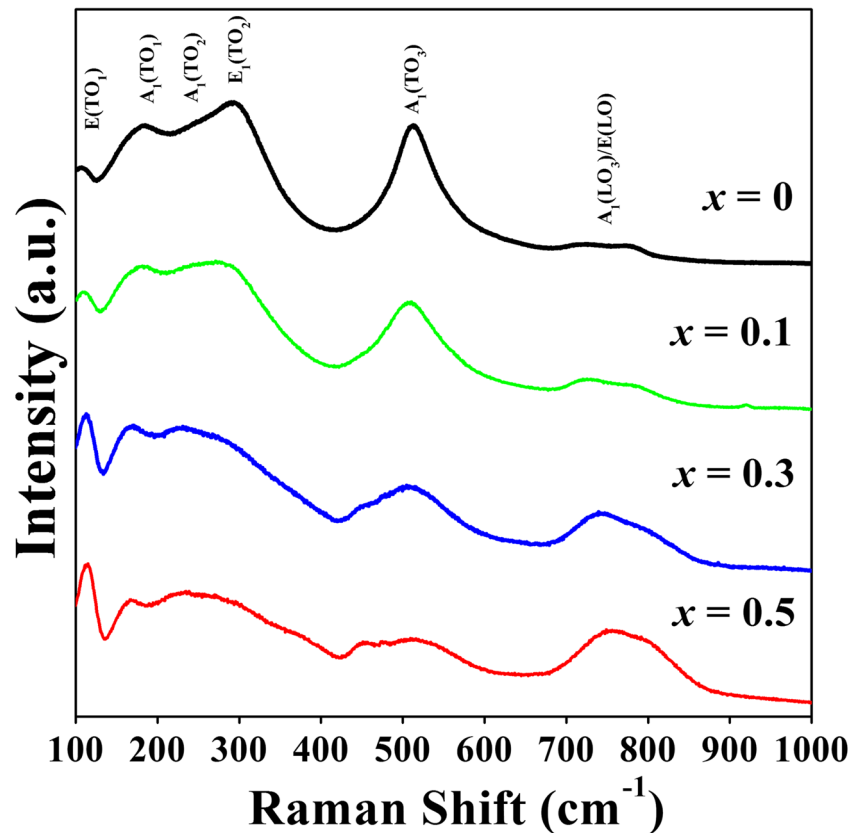
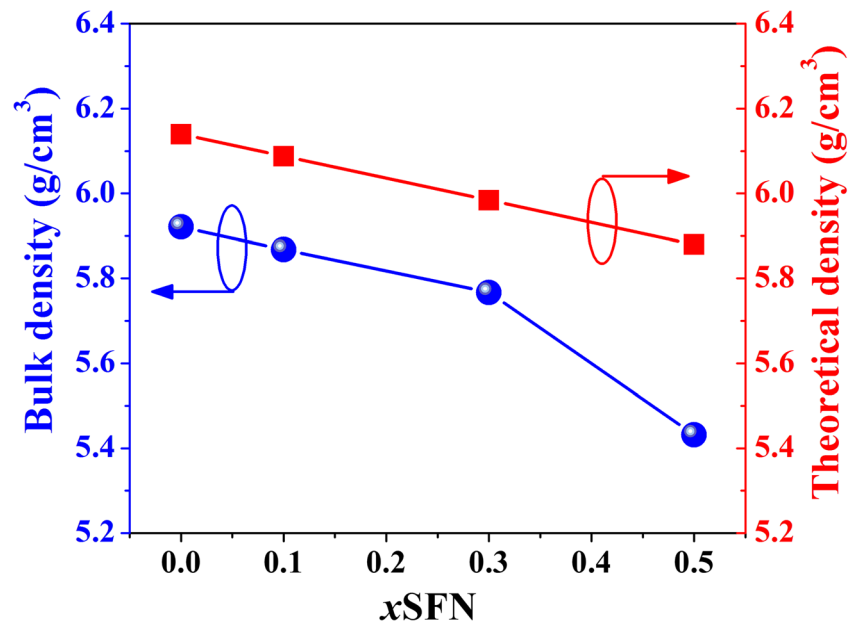


**Fig. 3** Plots of bulk density and theoretical density as a function of SFN content



curve where the measured density values are lower than those of the calculated densities. This may be due to the presence of close pores in the samples.

The characteristic temperature and frequency dependences of the dielectric constant for  $(1-x)\text{BZT}-x\text{SFN}$  ceramics are shown in Fig. 4. The dielectric constant curves for the unmodified ceramic present a diffuse phase transition around the transition temperature ( $T_m \sim -5^\circ\text{C}$ ). The dielectric curves also exhibit a weak dispersive dielectric behavior with respect to frequency. This characteristic indicates that the sample exhibits a ferroelectric behavior (at low temperatures) which is similar to many previous works [2, 3, 6, 7]. However, an obvious change in the dielectric behavior is noted for the solid-solution samples. For the  $x=0.1$  ceramic, flat dielectric constant curves are observed. However, the dielectric constant-temperature curves for the  $x=0.1$  ceramic do not show any peak. This is probably due to the temperature limit of the measurement. The  $x=0.1$  ceramic also presents a frequency dependence of the dielectric constant, especially for high temperatures. For the compositions of  $x \geq 0.3$ , the samples present plateaus with a stronger frequency dispersion of dielectric constant, especially for high temperatures. It should be noted that the dielectric constants of the  $x=0.3$  sample are quite high ( $\epsilon_r \sim 27,000$  for temperatures  $>150^\circ\text{C}$  and at 1 kHz). For the  $x=0.5$  sample, very high dielectric constants are recorded, i.e.  $\epsilon_r > 7000$  at  $\sim 30^\circ\text{C}$  and  $\epsilon_r > 164,000$  for temperatures  $>150^\circ\text{C}$  (at 1 kHz). The dielectric constant behavior for the  $x \geq 0.3$  samples is similar to the dielectric constant behavior of SFN ceramics and other well-known high dielectric constant ceramics such as  $\text{Ba}(\text{Fe}_{0.5}\text{Nb}_{0.5})\text{O}_3$  [23],  $\text{Ba}(\text{Fe}_{1/2}\text{Ta}_{1/2})\text{O}_3$  [12] and  $\text{CaCu}_3\text{Ti}_4\text{O}_{12}$  [14]. However, the dielectric constant for

the  $x=0.5$  ceramics are obviously high as compared to both BZT ( $\sim 4500$  @  $300\text{ K}$  and  $10\text{ kHz}$ ) [18] and SFN ( $\sim 5200$  @  $\text{RT}$  and  $10\text{ kHz}$ ) ceramics [15]. Figure 4 also displays dielectric loss ( $\tan \delta$ ) versus temperature at various frequencies and SFN concentrations. The dielectric loss data agrees well with the dielectric constant data. For the unmodified sample, the  $\tan \delta$  curves exhibit a weak frequency dispersion. For the  $x=0.1$  sample, the  $\tan \delta$  curves show a more pronounced frequency-dependent characteristic over a wide temperature range. For the  $x \geq 0.3$  samples, the  $\tan \delta$  curves present a stronger frequency-dependent characteristic. The peaks of  $\tan \delta$  shift to higher temperatures with increasing frequency. This behavior is similar to the dielectric loss behavior of SFN and other high dielectric ceramics [23]. Thus, a ceramic containing higher SFN concentration may exhibit relaxor-like dielectric behavior, but not for the well-known relaxors.

To check the ferroelectric behavior, polarization-electric ( $P$ - $E$ ) field measurement was employed at various temperatures. The hysteresis loops ( $P$ - $E$  loops) obtained from the measurement for selected studied ceramics are illustrated in Fig. 5. For the unmodified sample (at  $-40^\circ\text{C}$ ), the hysteresis loops present a near-square loop. Remnant polarization ( $P_r$ ) of  $6.4\ \mu\text{C}/\text{cm}^2$  and coercive field ( $E_c$ ) of  $2.1\ \text{kV}/\text{cm}$  are noted at this temperature. At temperatures above  $T_m$  (such as at  $30^\circ\text{C}$ ), the slim and slant hysteresis loops with non-zero of  $P_r$  value are displayed. The hysteresis result also agrees with the dielectric result, i.e. there is a diffuse phase transition at  $T_m$ . For the composition of  $x=0.1$ , it seems that the hysteresis loop exhibits non-square hysteresis loop which indicates that the ceramic has higher leakage current ( $I$ ). This result agrees with the higher values of  $\tan \delta$  for this composition ( $x=0.1$ ). Therefore, the  $x=0.1$  sample has a low resistance as

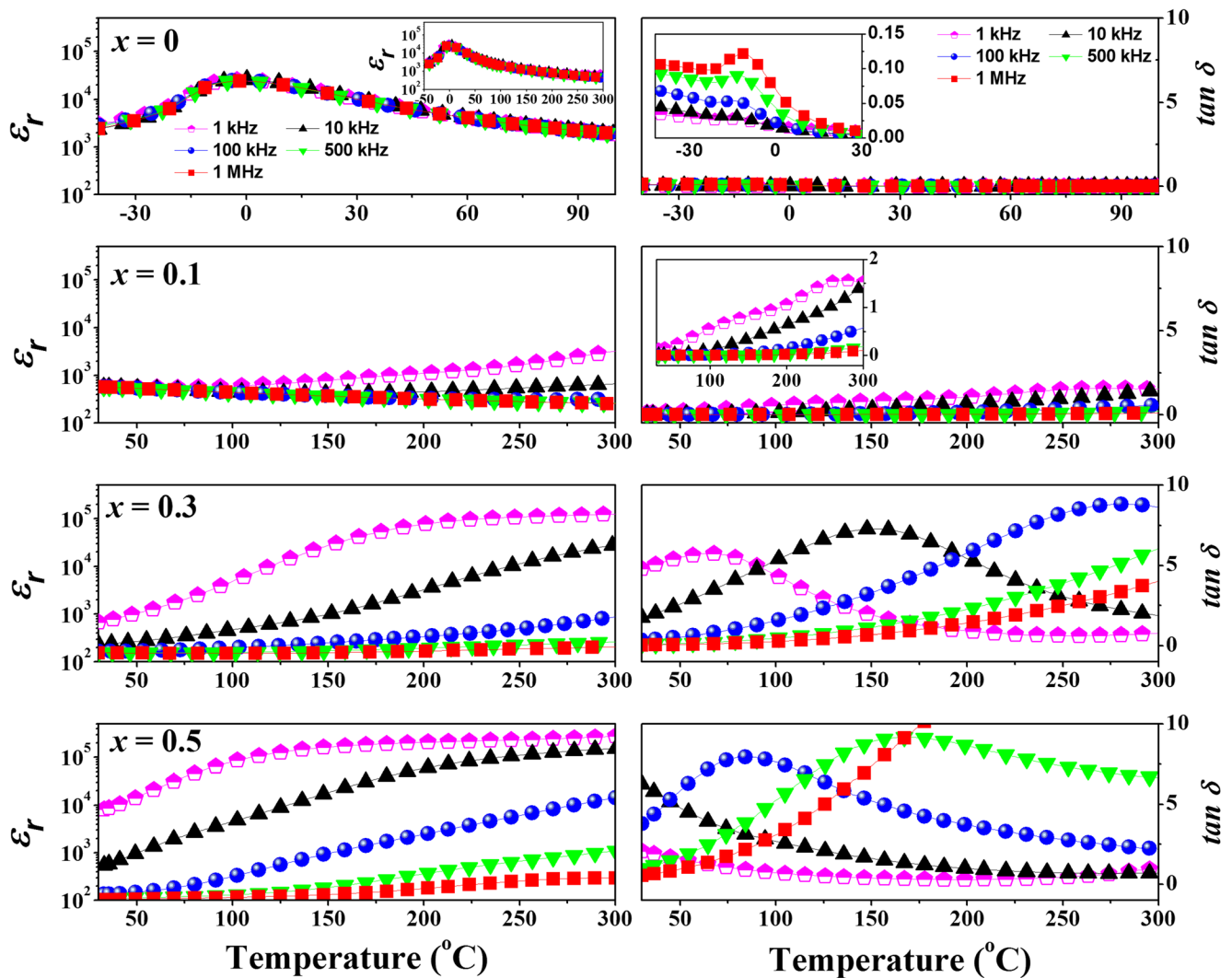


**Fig. 4** Dielectric constant ( $\epsilon_r$ ) and dielectric loss ( $\tan \delta$ ) as a function of temperature for  $(1-x)\text{BZT}-x\text{SFN}$  ceramics (Insets: magnify the curves at selected temperatures)

compared to the unmodified ceramic [8, 24]. For the  $x \geq 0.3$  ceramics, the hysteresis loop could not be obtained due to an electrical breakdown problem. This can be linked to the fact that the samples had higher leakage currents. To check this, the leakage current was measured. Plots of  $I$  versus applied electric field ( $E$ ) are displayed in Fig. 6. The values of  $I$  for the  $x = 0.1$  sample are higher than the unmodified ceramics, as expected. It is noted that the leakage current curve for the other samples could not be obtained due to the electrical breakdown problem.

To have a further understanding of the dielectric and ferroelectric behaviors, an impedance spectroscopy technique was employed. Imaginary part ( $Z''$ ) versus real part ( $Z'$ ) or  $Z^*$  plot of the impedance data for the studied ceramics was carried out. The  $Z^*$  plots for the studied ceramics at different temperatures are displayed in Fig. 7, while Fig. 8 displays  $Z^*$  plots for all ceramics at  $30^\circ\text{C}$ . For the unmodified ceramic ( $x = 0$ ), the  $Z^*$  plots at low and intermediate temperatures show a part

of a very big arc (with non-intercept). However, the diameter of the arcs decreases with increasing temperature. Furthermore, the arc seems to split into two arcs at high temperatures (such as at  $200^\circ\text{C}$ ). This suggests that resistivity which corresponds to the arc ( $R$ ) of the sample decreases with increasing temperature. Normally, the arcs in the  $Z^*$  plot can be likened to many effects such as bulk grain and grain boundary responses, where resistance of each response can be estimated from the curve intercept (at  $Z'$  axis) [25, 26]. By using an equivalent parallel resistance-capacitance ( $RC$ ) circuit model, a semicircular arc can be obtained from the  $Z^*$  plot, where  $C$  is specific capacitance (in unit of  $\text{F}\cdot\text{cm}^{-1}$ ) for each arc which can be linked with each response. The  $C$  value for each response (each arc) can be determined from the equation:  $2\pi f_{\max} CR = 1$ , where  $f_{\max}$  is frequency at which  $Z''$  reaches its maximum value for the consideration arc [25, 26]. By using hand fitting of the data for the  $200^\circ\text{C}$  arc at high frequency region,  $R$  and  $C$  values are approximated to be  $6.2 \times 10^6 \Omega\cdot\text{cm}$

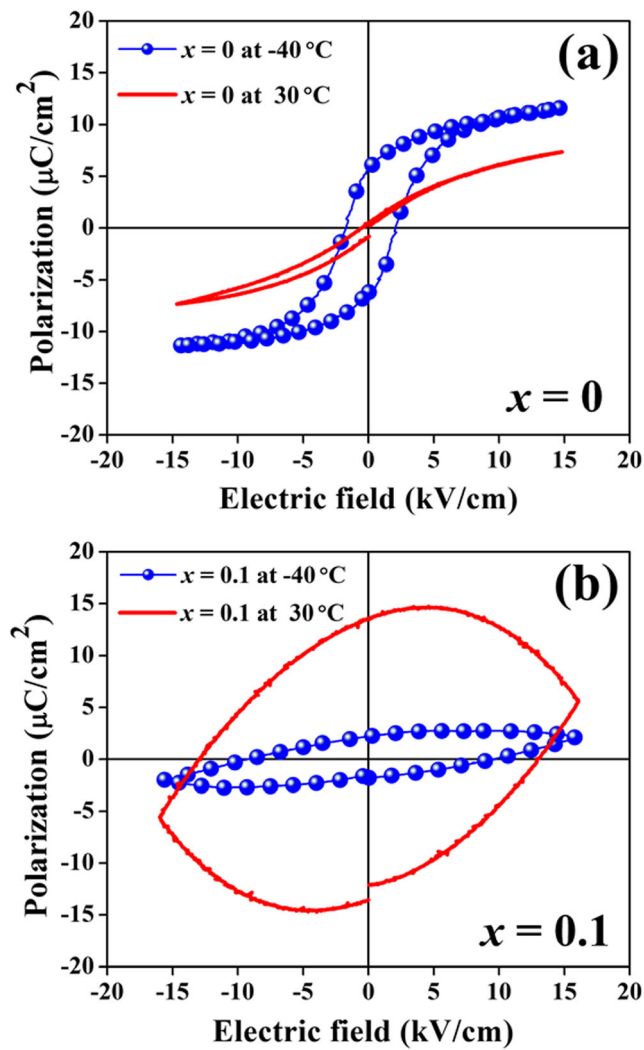


Fig. 5 Selected  $P$ - $E$  hysteresis loops at  $-40$  and  $30$  °C for  $(1-x)$ BZT- $x$ SFN ceramics where (a)  $x = 0$  and (b)  $x = 0.1$

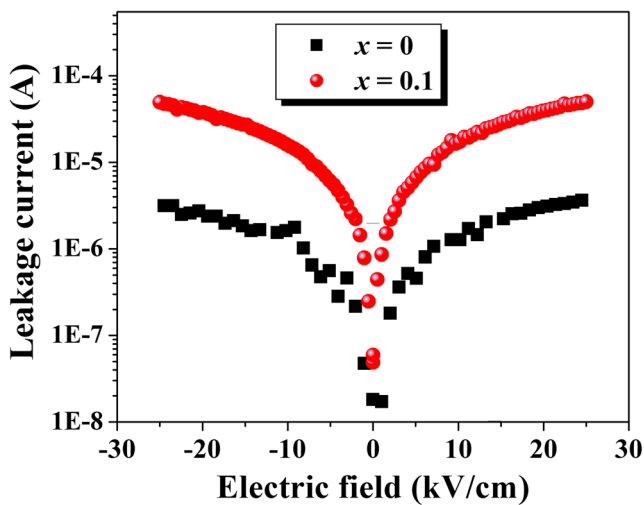


Fig. 6 Plot of leakage current as a function of electric field of  $(1-x)$ BZT- $x$ SFN ceramics where  $x = 0$  and  $0.1$

and  $8.1 \times 10^{-11} \text{ F.cm}^{-1}$ , respectively. The capacitance value is between capacitance values of bulk grain and grain boundary responses [27]. For the  $0.1 \leq x \leq 0.3$  ceramics, the  $Z^*$  plots present the same trend as being in the unmodified ceramic. The  $R$  and  $C$  values for the  $x = 0.1$  ceramic could not be determined due to the presence of unclear arcs on the  $Z^*$  curves. In case of the  $x = 0.3$  ceramic, however, the  $R$  values at  $-40, 30, 100, 200^\circ\text{C}$  arcs are  $8.9 \times 10^6, 5.6 \times 10^5, 6.9 \times 10^4$  and  $1.1 \times 10^4 \Omega.\text{cm}$  while  $C$  values are  $2.3 \times 10^{-11}, 1.8 \times 10^{-11}, 1.7 \times 10^{-11}$  and  $1.2 \times 10^{-11} \text{ F.cm}^{-1}$ , respectively. The capacitance values of this ceramic are also between the capacitance values of bulk grain and grain boundary responses. Therefore, it is believed that many responses may have contributed to the dielectric behavior. For the  $x = 0.5$  ceramic, the  $Z^*$  plots show three arcs (at some temperatures), including a big arc with no intercept at low frequency region, an arc at high frequency region, and a small arc at intermediate frequency region (indicated by \*) which overlaps with the low and high frequency arcs (see also Fig. 8). The presence of these three arcs indicates that the dielectric behavior for this sample should be associated with many responses. The  $R$  values which are associated to  $-40$  and  $30^\circ\text{C}$  arcs are  $6.5 \times 10^5$  and  $4.26 \times 10^4 \Omega.\text{cm}$  while  $C$  values are  $9.8 \times 10^{-12} \text{ F.cm}^{-1}$  and  $9.9 \times 10^{-12} \text{ F.cm}^{-1}$ , respectively. However, these values could not be determined from the  $100$  and  $200^\circ\text{C}$  curves due to the incomplete arc problem. This suggests that addition of SFN produces a reduction in resistance of the bulk grain.

To check the effects occurring in the ceramic, plots of  $Z''$  versus frequency ( $Z''-f$ ) were carried out, as seen in Fig. 9. It seems that the  $Z''-f$  plots for the unmodified ceramic at  $-40$  to  $100^\circ\text{C}$  present a part of  $Z''$  peak of the  $Z''-f$  curve. However, a peak of  $Z''-f$  curve is noted at  $200^\circ\text{C}$ . The  $R$  and  $C$  values which correspond to the peak were estimated by using the equations:  $R = 2Z''$  and  $2\pi fRC = 1$  [26, 28]. The  $R$  and  $C$  values which correspond to the peaks of the  $200^\circ\text{C}$  curve are  $7.2 \times 10^6 \Omega.\text{cm}$  and  $6.1 \times 10^{-11} \text{ F.cm}^{-1}$ , respectively. This result agrees with the  $Z^*$  result. For the  $x = 0.1$  ceramic, peaks of  $Z''-f$  plots are noted at high temperatures (such as  $100$  and  $200^\circ\text{C}$ ). The  $R$  values associated with the peaks for  $100$  and  $200^\circ\text{C}$  curves are  $3.0 \times 10^6 \Omega.\text{cm}$  and  $2.3 \times 10^4 \Omega.\text{cm}$ , while  $C$  values are  $2.7 \times 10^{-11} \text{ F.cm}^{-1}$  and  $1.6 \times 10^{-11} \text{ F.cm}^{-1}$ , respectively. For the  $x = 0.3$  ceramic, peaks of  $Z''-f$  plots are noted at intermediate temperatures (such as  $30^\circ\text{C}$ ) and also high temperatures (such as  $100$  and  $200^\circ\text{C}$ ). The  $R$  values associated with the peaks for  $30, 100,$  and  $200^\circ\text{C}$  curves are  $2.6 \times 10^5, 2.7 \times 10^4,$  and  $4.2 \times 10^3 \Omega.\text{cm}$ , while  $C$  values are  $1.8 \times 10^{-11}, 1.5 \times 10^{-11}$  and  $1.2 \times 10^{-11} \text{ F.cm}^{-1}$ , respectively. This corresponds to the result from  $Z^*$  plots. For the  $x = 0.5$  ceramic,  $Z''-f$  plots display clear peaks at some temperatures such as at  $-40$  and  $30^\circ\text{C}$ . The  $R$  values associated with the peaks for  $-40$  and  $30^\circ\text{C}$  curves are  $2.8 \times 10^5,$  and  $2.2 \times 10^4 \Omega.\text{cm}$ , while  $C$  values are  $9.8 \times 10^{-12}$  and  $7.6 \times 10^{-12} \text{ F.cm}^{-1}$ , respectively [29]. These peaks should be associated with bulk grain response.

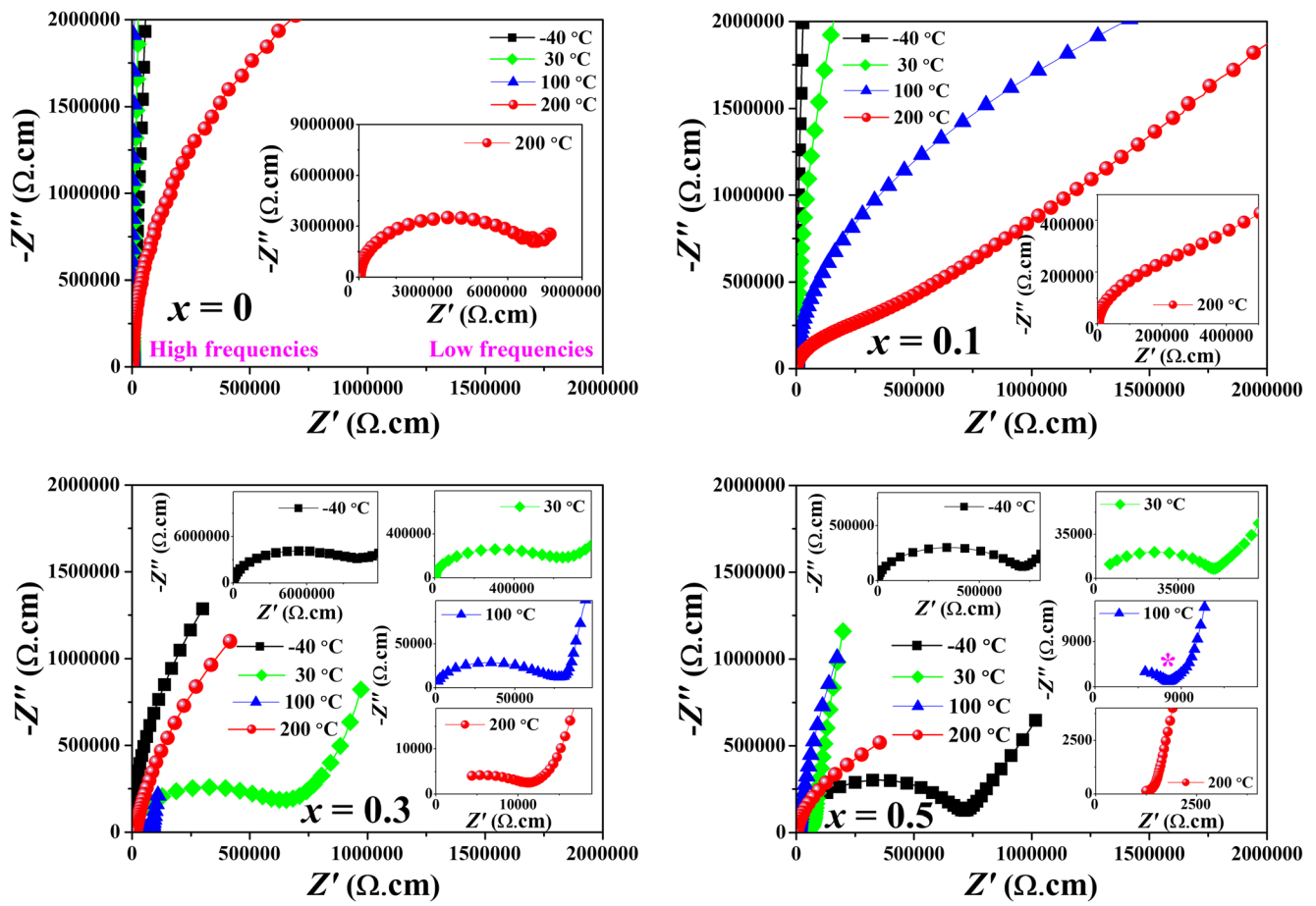
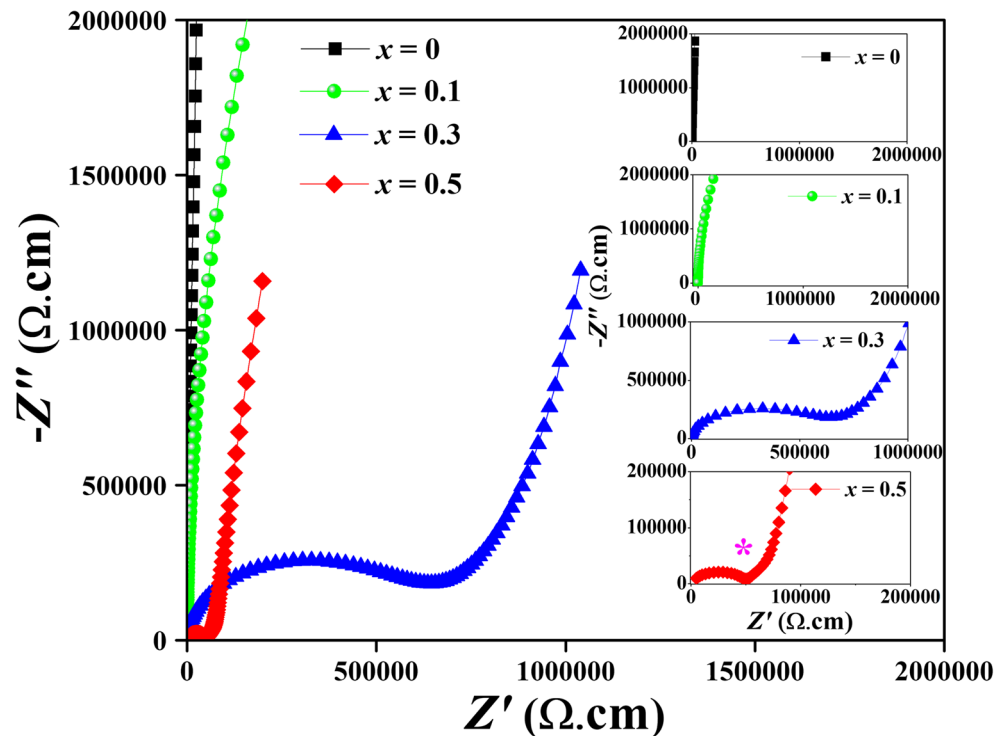


Fig. 7 Plots of  $Z'$  and  $Z''$  of  $(1-x)\text{BZT}-x\text{SFN}$  ceramics measured at different temperatures where  $x = 0, 0.2, 0.3$  and  $0.5$

Fig. 8 Plots of  $Z'$  and  $Z''$  of  $(1-x)\text{BZT}-x\text{SFN}$  ceramics measured at  $30^\circ\text{C}$  (Insets: magnify of each composition)



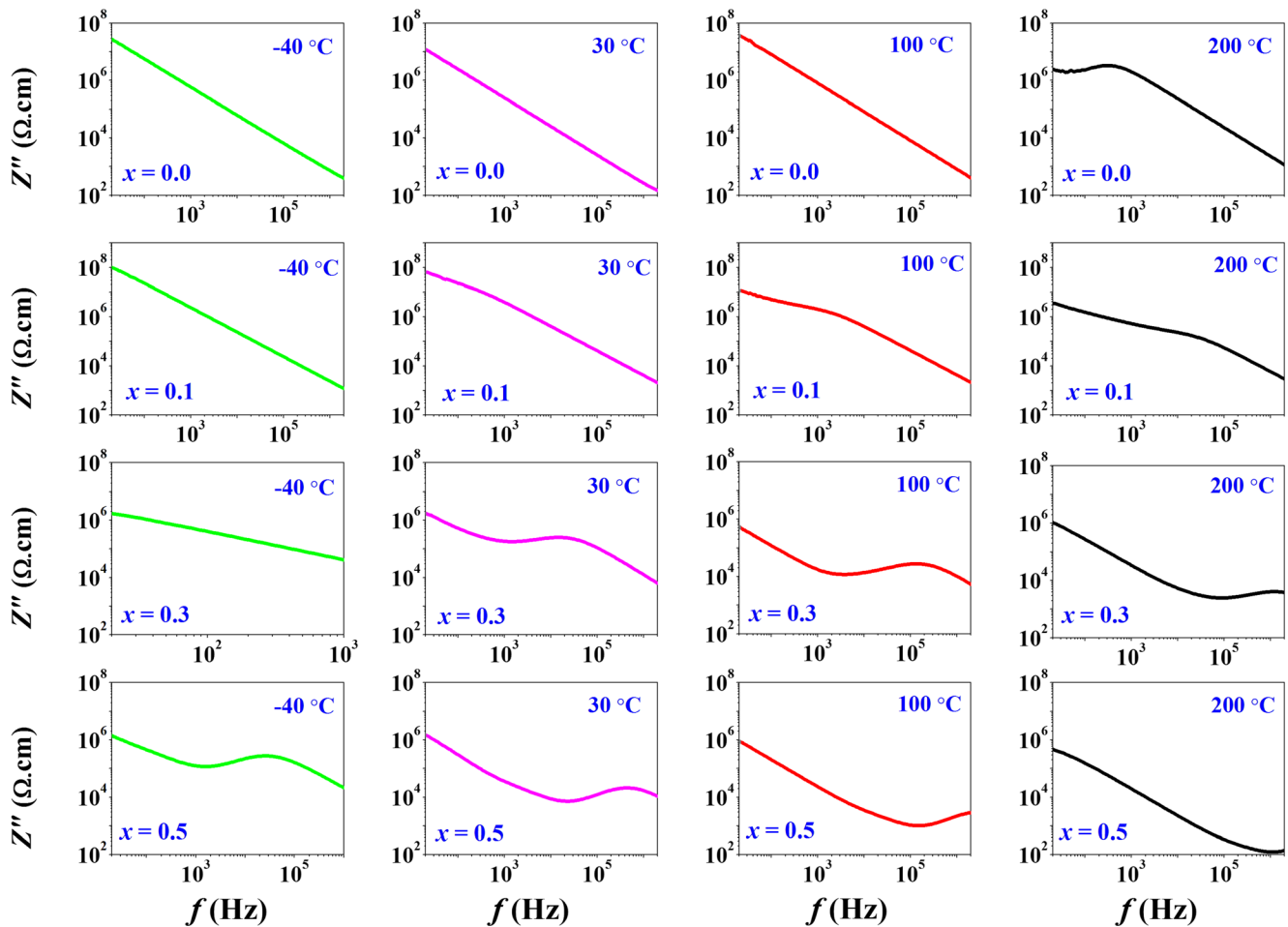


Fig. 9 Plots of  $Z''$  versus  $f$  ( $Z''-f$ ) of  $(1-x)$ BZT- $x$ SFN ceramics measured at different temperatures where  $x = 0, 0.2, 0.3$  and  $0.5$

Furthermore, the presence of three arcs on  $Z^*$  plots suggests that other effects such as grain boundary and sample-electrode interface responses should contribute to the dielectric behavior. However, there is no clear evidence obtained from the  $Z''-f$  plots.

To further verify that these effects occurred, plots of  $C$  versus  $f$  [29] were carried out as seen in Fig. 10. The  $C-f$  curves for the unmodified ceramic show a flat straight line (plateau) type, except for the curve at 200°C (it seems that the 200°C curve is going to show another plateau at low frequencies). The  $C-f$  curves for the  $x = 0.1$  ceramic present curves with unclear plateau (the plateaus could not be clearly observed at low frequencies due to the limit of the instrument). However, at low temperatures such as at -40 °C, the  $C-f$  curve exhibits a flat straight line. For the  $x = 0.3$  ceramic, the  $C-f$  curves present dielectric constant plateaus especially at high temperatures. An approximate  $C$  value for this plateau (at  $\sim 10^1-10^2$  Hz and 200°C) is  $\sim 10$  nF.cm<sup>-1</sup>. The dielectric behavior for this sample should be associated with many responses such as bulk grain and grain boundary. For the  $x = 0.5$  ceramic at low temperatures (such as -40°C), only one clear capacitance plateau is noted at intermediate and high

frequencies. An approximate  $C$  value for this plateau (at  $\sim 10^4-10^6$  Hz and -40°C) is  $\sim 9$  pF.cm<sup>-1</sup>. This plateau should be associated with bulk grain response. At 30°C and 100°C, it seems that the curves show two plateaus at low and intermediate frequencies. At 200°C, the curve shows two capacitance plateaus (indicated by  $\nabla$ ) and another incomplete plateau (at high frequencies). An approximated  $C$  values at low frequency plateau (at  $\sim 10^1-10^2$  Hz) is  $\sim 17$  nF.cm<sup>-1</sup>, while the approximated  $C$  values at the intermediate frequency plateau (at  $\sim 10^3-10^4$  Hz) is  $\sim 10$  nF.cm<sup>-1</sup>. The capacitance plateaus at low frequencies should be associated with sample-electrode interface response while the capacitance plateaus at intermediate frequencies should be associated with grain boundary response [29, 30].

Normally, the electrical behavior of many high dielectric ceramics can be explained in terms of the Maxwell-Wagner mechanism which can be linked with the formation of Schottky barrier due to a mismatch of Fermi energy levels between different conduction regions such as semiconducting grain and insulating grain boundary [29, 30]. This can produce the dielectric constant-frequency dispersion with high dielectric constants at some frequencies, where this behavior is not



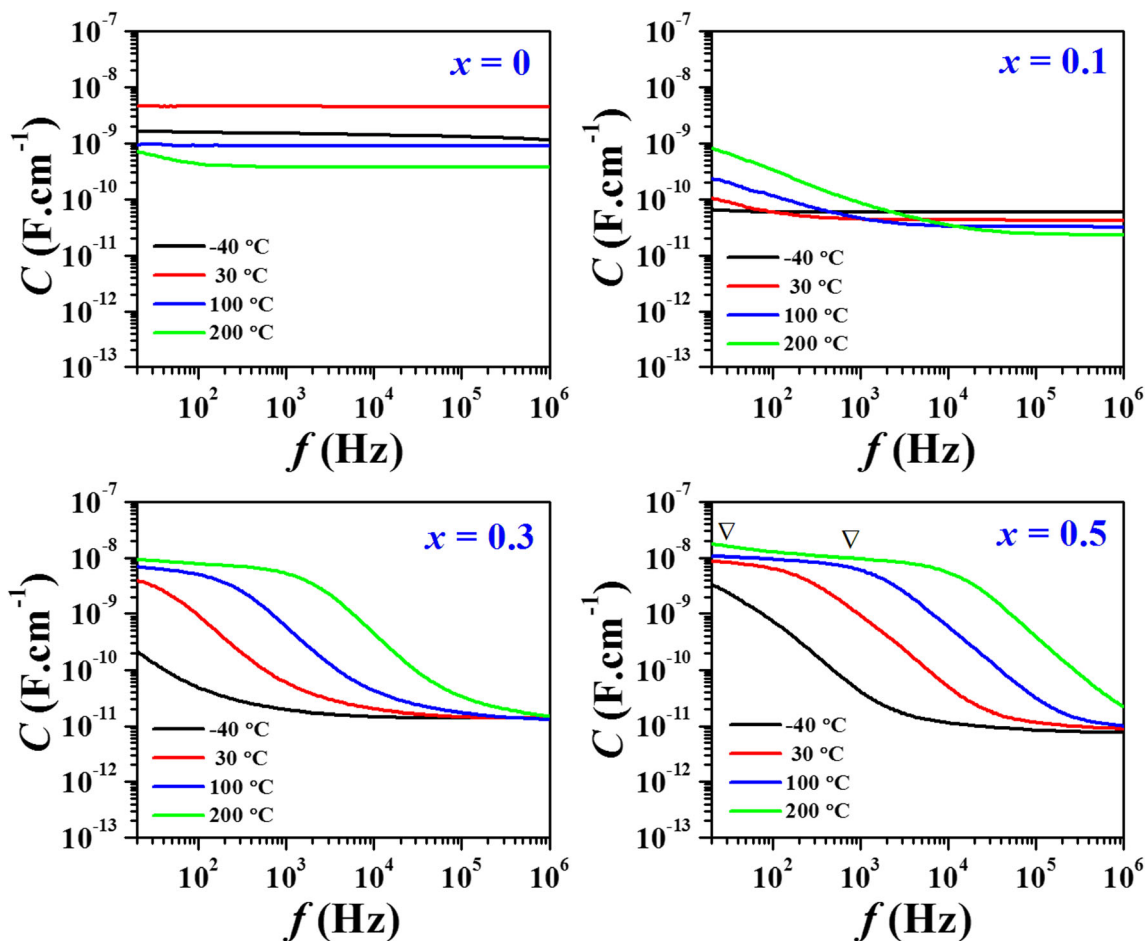


Fig. 10 Plots of  $C$  versus  $f$  of  $(1-x)\text{BZT}-x\text{SFN}$  ceramics measured at different temperatures where  $x = 0, 0.2, 0.3$  and  $0.5$

necessarily associated with ferroelectricity [28]. In the case of the unmodified ceramic, the dielectric behavior should be affected by ferroelectric response. This can be confirmed by the presence of ferroelectric hysteresis loops (especially at low temperature). In the case of the  $x = 0.1$  ceramic, other responses start to present while in the case of the  $x = 0.3$  ceramic, many responses such as grain boundary response has a bigger for the dielectric behavior as evidenced by the clear dielectric constant-frequency dispersion (as compared to the  $x = 0.1$  ceramic, also seen Fig. 4). In the case of  $x = 0.5$  ceramic, the bulk grain has low resistivity, as evidenced by the greatly reduced diameter of the arc at high frequency for the  $Z^*$  plot. The conduction mechanism for the bulk grain of this ceramic should be related with the formation of multivalence ions such as  $\text{Fe}^{2+}/\text{Fe}^{3+}$  after the solid solution of BZT-SFN was formed, where electron hopping mechanism between the multivalence ions can result in the reduction of resistivity [30, 31]. Based on the obtained data, the dielectric behavior of the  $x = 0.5$  ceramic sample should be affected by many responses such as bulk grain and grain boundary responses. Other responses such as sample-electrode interface should also contribute to the dielectric behavior of the  $x = 0.5$  ceramic, especially at high temperatures and low frequencies. This,

therefore, can produce a higher degree of dielectric constant-frequency dispersion or relaxor-like dielectric behavior with very high dielectric constants, as compared to other ceramic samples.

## 4 Conclusion

Effects of SFN on the properties of  $(1-x)\text{BZT}-x\text{SFN}$  ceramics have been investigated. The ceramics have been fabricated via a solid-state reaction technique. All ceramics have a pure phase perovskite structure at RT. A small amount of SFN addition ( $x = 0.1$ ) produces an obvious change in the dielectric behavior. The further addition of SFN enhances dielectric constants of the solid solution, especially for ceramics containing a higher SFN concentration. The  $x = 0.5$  ceramics present very high dielectric constants as compared to the other studied samples and also other dielectric materials. The complex impedance spectroscopy analysis indicates that the  $x \geq 0.1$  ceramics are affected by many responses such as bulk grain and grain boundary or the ceramics having heterogeneous conduction. Combined with the dielectric, ferroelectric, and impedance data, the addition of SFN produces a transformation from

a ferroelectric behavior to a relaxor-like dielectric behavior for the studied ceramic system.

**Acknowledgements** This work was supported by the Thailand Research Fund (TRF, BRG 6080002, IRG5780013), National Research University Project under Thailand's Office of the Higher Education Commission, 50<sup>th</sup> CMU anniversary Ph.D. Program Chiang Mai University. Department of Physics and Materials Science, Faculty of Science and Graduate School, Chiang Mai University, Thailand is also acknowledged.

## References

- J.Q. Qi, B.B. Liu, H.Y. Tian, H. Zou, Z.X. Yue, L.T. Li, *Solid State Sci.* **14**, 1520–1524 (2012).
- Z. Yu, C. Ang, R. Guo, A.S. Bhalla, *Mater. Lett.* **61**, 326–329 (2007)
- T. Maiti, R. Guo, A.S. Bhalla, *J. Am. Ceram. Soc.* **91**, 1769–1780 (2008)
- Z. Yu, C. Ang, R. Guo, A.S. Bhalla, *J. Appl. Phys.* **92**, 1489–1493 (2002)
- P. Jarupoom, K. Pengpat, G. Rujijanagul, *Curr. Appl. Phys.* **10**, 557–560 (2010)
- X.G. Tang, K.H. Chew, H.L.W. Chan, *Acta Mater.* **52**, 5177–5183 (2004)
- S. Ke, H. Fan, H. Huang, H.L.W. Chan, S. Yu, *Phys. Lett.* **104**, 034108 (2008)
- C. Kruea-In, S. Eitssayeam, K. Pengpat, G. Rujijanagul, *Mater. Res. Bull.* **47**, 2859–2862 (2012)
- Y.Y. Liu, X.M. Chen, X.Q. Liu, L. Li, *Appl. Phys. Lett.* **90**, 192905 (2007)
- S. Saha, T.P. Sinha, *J. Appl. Phys.* **99**, 014109 (2006)
- Z. Wang, X.M. Chen, L. Ni, X.Q. Liu, *Appl. Phys. Lett.* **90**, 022904 (2007)
- A. Dutta, T.P. Sinha, *Mat. Res. Bull.* **46**, 518–524 (2011)
- X. Lv, X.Q. Liu, H.J. Zhao, W.Z. Yang, X.M. Chen, *J. Am. Ceram. Soc.* **96**, 1188–1192 (2013).
- M. Li, D.C. Sinclair, A.R. West, *J. Appl. Phys.* **109**, 084106 (2011)
- T. Phatungthane, G. Rujijanagul, *Ceram. Int.* **41**, 2968–2975 (2015)
- P. Jarupoom, G. Rujijanagul, *J. Appl. Phys.* **114**, 027018 (2013)
- S. Yao, W. Ren, H. Ji, X. Wu, P. Shi, D. Xue, X. Ren, Z.G. Ye, *J. Phys. D. Appl. Phys.* **45**, 195301 (2012)
- T. Badapanda, S.K. Rout, L.S. Cavalcante, J.C. Sczancoski, S. Panigrahi, E. Longo, M.S. Li, *J. Phys. D. Appl. Phys.* **42**, 175414 (2009)
- R.D. Shannon, *Acta Cryst* **A32**, 751–767 (1976)
- P.S. Dobal, A. Dixit, R.S. Katiyara, Z. Yu, R. Guo, A.S. Bhalla, *J. Appl. Phys.* **89**, 8085–8091 (2001)
- F. Moura, A.Z. Simoes, L.S. Cavalcante, M.A. Zaghete, J.A. Varela, E. Longo, *J. Alloy, Compd.* **466**, L15–L18 (2008)
- L.S. Cavalcante, M. Anicete-Santos, J.C. Sczancoski, L.G.P. Simoes, M.R.M.C. Santos, J.A. Varela, P.S. Pizani, E. Longo, *J. Phys. Chem. Solids* **69**, 1782–1789 (2008)
- U. Intatha, S. Eitssayeam, J. Wang, T. Tunkasiri, *Curr. Appl. Phys.* **10**, 21–25 (2010)
- P. Jaita, P. Butnoi, R. Sanjoom, C. Randorn, R. Yimmirun, G. Rujijanagul, *Ceram. Int.* **43**, S2–S9 (2017)
- M. Li, A. Feteira, D.C. Sinclair, *J. Appl. Phys.* **98**, 084101 (2005)
- F.D. Morrison, D.C. Sinclair, A.R. West, *J. Am. Ceram. Soc.* **84**, 531–538 (2001)
- J.T.S. Irvine, D.C. Sinclair, A.R. West, *Adv. Mater.* **2**, 132–138 (1990)
- M. Li, D.C. Sinclair, *J. Appl. Phys.* **111**, 054106 (2012)
- M. Li, A. Feteira, D.C. Sinclair, *J. Appl. Phys.* **105**, 114109 (2009)
- J.G. Lopez, N. Maso, B. Levenfeld, A. Varez, A.R. West, *J. Am. Ceram. Soc.* **99**, 2327–2333 (2016)
- S. Ananta, N.W. Thomas, *J. Eur. Ceram. Soc.* **19**, 1873–1881 (1999)